IOP Publishing Superconductor Science and Technology
Supercond. Sci. Technol. 31 (2018) 025006 (16pp) https://doi.org/10.1088/1361-6668/aa9dc1

Superconducting magnetic bearings with bulks and 2G HTS stacks: comparison between simulations using H and A-V formulations with measurements

F Sass[1,3], D H N Dias[1], G G Sotelo[1] and R de Andrade Junior[2]

[1] Department of Electrical Engineering, Universidade Federal Fluminense, Niterói, Rio de Janeiro, Brazil
[2] Department of Electrical Engineering, Universidade Federal do Rio de Janeiro, Rio de Janeiro, Rio de Janeiro, Brazil

E-mail: felipesass@id.uff.br, dhndias@id.uff.br, gsotelo@id.uff.br and rubens.andrade.jr@poli.ufrj.br

Received 13 September 2017, revised 1 November 2017
Accepted for publication 28 November 2017
Published 4 January 2018

Abstract

A-V and H are two of the most widespread formulations applied in the literature to calculate current distribution in high-temperature superconductors (HTSs). Both formulations can successfully solve problems related to large-scale HTS applications, but the way to implement the calculations is different. In recent years, several authors have chosen the H formulation to solve problems related to HTS applications. This choice can probably be attributed to the easy implementation of the H formulation with the aid of commercial finite element method (FEM) software, producing precise results and performing fast calculations. In a previous work, we proposed the use of the H formulation to solve superconducting magnetic bearing (SMB) problems. However, most of the SMB simulations presented in the literature are solved using the A-V formulation implemented with the finite difference method (FDM). Which of these two techniques is more suitable for superconducting magnetic bearing applications? This paper aims to answer this question. In order to do so, an experimental rig was developed to test SMBs using YBCO bulks or stacks of coated conductors. The simulated levitation force results from the A-V formulation using FDM and from the H formulation using FEM were compared with the experimental data. In general, the calculation time and the results error obtained with both formulations are comparable. It is worth mentioning that the main contribution of this paper is to present improvements to reduce the A-V formulation computational time and details of how to implement it using FDM in any platform. For this reason, most of this work is about the A-V formulation, while the H formulation is just presented for comparison.

Keywords: H formulation, A-V formulation, simulation of superconductors, superconducting magnetic bearings, superconducting levitation, coated conductors

(Some figures may appear in colour only in the online journal)

1. Introduction

High-temperature superconductors (HTSs) have the potential to be used in several large-scale applications [1]. For the general public, superconducting levitation is the HTS application that catches the eye. In terms of practical interest for industry and for society, superconducting levitation can be applied to develop rotational [2, 3] and linear [4, 5] superconducting magnetic bearings (SMBs). Rotational SMBs can be applied to high-speed spinning shafts (over 20 000 RPMs) and flywheel energy storage systems, while linear SMBs are used in maglev vehicles. Usually, an SMB is composed of a

[3] Author to whom any correspondence should be addressed.

magnetic field produced by a permanent magnet (PM) and HTS bulk material. More recently, the quality improvements presented by coated conductors has motivated several groups to study the replacement of HTS bulks with stacks of second generation (2G) tapes in SMB applications [6, 7].

One of the most important parameters in an SMB is the magnetic force that appears due to the interaction between the superconductor and the PM. The unusual characteristic of this force gives the system unique levitation properties. One well known method for determining its behaviour consists of finding the current distribution inside the HTS. The literature presents several physical formulations to calculate the current distribution inside the HTS: the H [8, 9], the A-V (or A-ϕ) [10–12], the T-ω [13, 14] and the E [15] formulations. Each formulation can be solved by different techniques such as the finite element method (FEM) and the finite difference method (FDM). The application of the H formulation and FEM to solve SMB with bulk superconductors and stacks of 2G tapes has previously been presented by the authors [16]. Here, this study is continued by also calculating the SMB levitation force with the A-V formulation and FDM. We present the details about the implementation of the A-V formulation, including a new method to obtain the matrices for the solution of the problem using analytical equations. The applied methodology speeds up the convergence of the problem. In the present study, A-V and H formulations were compared for several studied cases, always presenting the respective levitation force measurement for comparison. In all cases, the calculation time and the error obtained by both formulations were at the same level. We concluded that both formulations could be used to solve the SMB problem.

In this manuscript, the H formulation was implemented with the aid of COMSOL, which is a commercial software based on FEM. On the other hand, the A-V formulation results were obtained using a self-written code in MATLAB. In general, writing all your own code gives you the advantage of being able to access any stage of the solution process. This is an important tool for dealing with any convergence problems.

Despite the fact that we are presenting results achieved using both H and A-V formulations, the original contribution of this work is the analytical equations that speed up the A-V formulation solution. In this way, most of the following text is about this technique. If the reader is more interested in the H formulation implementation using COMSOL for computing the superconducting levitation force, [16] this is a good point to start.

2. Methodology

This section presents information about SMB modeling, including how the external magnetic field produced by the permanent magnets was computed, the way in which the 2G HTS stacks are represented, and a description of the adopted experimental procedures.

2.1. Modeling of the superconducting magnetic bearings by A-V formulation

Superconducting magnetic bearings are usually composed of two parts: a PM (or a PM array) and the HTS. The PM is responsible for producing the external magnetic field, while the HTS will react to any magnetic field change in order to reach stable levitation at all degrees of freedom, except in the direction where there is free movement without friction losses.

Usually, the A-V formulation is modeled in the FEM software by constituent equation (1):

$$\mu\,\sigma\,\frac{\partial \mathbf{A}}{\partial t} - \nabla \times \nabla \times \mathbf{A} = -\mu\,\sigma\,\nabla V. \tag{1}$$

However, when we say A-V formulation in this work, we mean that the magnetic vector potential ($\mathbf{A}$) and the electric scalar potential (V) were used to determine the electric field ($\mathbf{E}$) in the HTS. In the sequence, the error of this result was minimized with an algorithm where the solution is the state variable current density ($\mathbf{J}$). To avoid misunderstandings, let us start from the very beginning: in electromagnetics theory, the magnetic vector potential is given by:

$$\mathbf{B} = \nabla \times \mathbf{A}. \tag{2}$$

Faraday's law $\left(\nabla \times \mathbf{E} = -\frac{\partial \mathbf{B}}{\partial t}\right)$ can be combined with equation (2), resulting in:

$$\mathbf{E} = \mathbf{E}_{\text{induced}} + \mathbf{E}_{\text{source}} = -\frac{\partial \mathbf{A}}{\partial t} - \nabla V; \tag{3}$$

where the total electrical field was decomposed into two parts:

- $\mathbf{E}_{\text{induced}}$—This variable represents the induced electric field due to time variations in the magnetic vector potential.
- $\mathbf{E}_{\text{source}}$—This variable represents the influence of electrical sources on the simulation domain.

The electric field and the magnetic vector potential in a model with 2D longitudinal symmetry in the z direction present only one non-null component: $\mathbf{E} = (0, 0, E_z)$ and $\mathbf{A} = (0, 0, A_z)$, respectively. Since $\mathbf{E}_{\text{source}} = -\nabla V$, we can also claim that $\nabla V = (0, 0, \partial V/\partial z)$ [17]. If the value of $\partial V/\partial z$ is defined in an arbitrary time instant as $C(t_n)$, equation (3) can be rewritten as:

$$E_z(x, y, t_n) = -\frac{\partial (A_z(x, y, t_n))}{\partial t} - C(t_n) \tag{4}$$

where C is a constant that must be defined in each domain as a function of the desired net current for a determined time instant. In passive SMB, the net current in the HTS cross-sectional area must be null. This naturally happens when the superconductor sample is in the presence of a symmetric magnetic field, so that the value of the C constant is zero. Illustrating this comment, figure 1 shows the four HTS domains using a symmetry axis. It is important to note that two of these domains are subject to a nonsymmetric magnetic field, so that the induced net current due to magnetic field variations will not be zero. For these cases, this paper presents

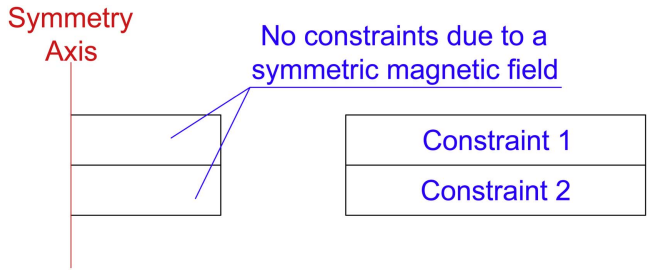

Figure 1. The illustration of a simulation with the four HTS domains using a symmetry axis. The current constraints are indicated.

an algorithm that finds the value of C to apply the desired net current in an HTS domain.

The total magnetic vector potential can be decomposed in the two following components:

$$A_z(x, y, t_n) = A_z^{\mathrm{EXT}}(x, y, t_n) + A_z^{\mathrm{HTS}}(x, y, t_n), \tag{5}$$

where A_z^{EXT} is the A_z component produced by the magnetic field sources external to the superconductor, and A_z^{HTS} is the A_z component produced by the HTS-induced currents. The development of the analytical equations to compute A_z^{EXT} and A_z^{HTS} is presented in the following sections. In analogy, the magnetic field intensity can be decomposed in:

$$H_x(x, y, t_n) = H_x^{\mathrm{EXT}}(x, y, t_n) + H_x^{\mathrm{HTS}}(x, y, t_n); \tag{6a}$$

$$H_y(x, y, t_n) = H_y^{\mathrm{EXT}}(x, y, t_n) + H_y^{\mathrm{HTS}}(x, y, t_n). \tag{6b}$$

Since $E_z = \rho J_z$, where ρ is the resistivity of the HTS sample, equation (4) can be combined with equation (5), resulting in

$$\rho(J_z)J_z(x, y, t_n) = -\frac{\partial A_z^{\mathrm{EXT}}(x, y, t_n)}{\partial t} - \frac{\partial A_z^{\mathrm{HTS}}(x, y, t_n)}{\partial t} - C(t_n). \tag{7}$$

In equation (7), the resistivity ρ is a function of J_z. This relation can be derived from the power law [18]:

$$\rho = \frac{E_c}{E_z}\left|\frac{J_z}{J_c}\right|^{n-1}, \tag{8}$$

where $E_c = 1\ \mu\mathrm{V\ cm^{-1}}$ for the definition. In this work, the variables J_c and n were modeled considering an exponential dependence of those parameters on the magnetic field [16, 19]:

$$J_c = J_{c_0}\exp\left(-\frac{|\mathbf{H}|}{H_J}\right), \tag{9a}$$

$$n = n_0\exp\left(-\frac{|\mathbf{H}|}{H_n}\right), \tag{9b}$$

where J_{c_0}, H_J, n_0 and H_n are the fitting parameters usually obtained from experimental measurements. Equations (9a) and (9b) need the magnetic field information provided by equations (6a) and (6b). In summary, the A-V formulation as presented in this work consists of using equation (7) to determine the J_z value in all points of the simulation domain.

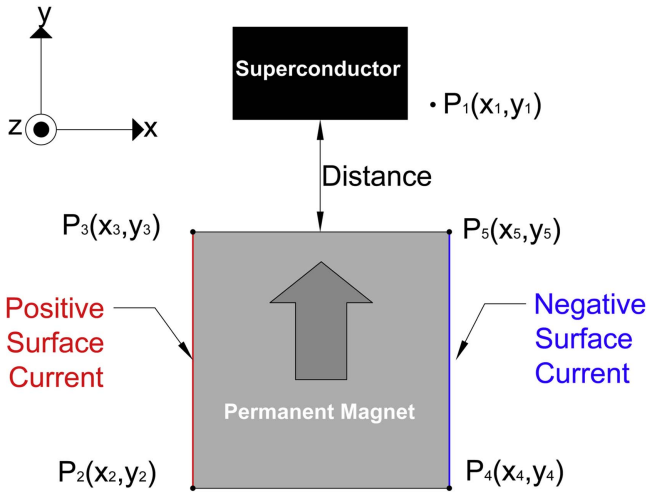

Figure 2. An illustration of the SMB studied in this work; the PM was modeled by two surface currents.

Details about the solution procedures using FDM will be presented.

After achieving a solution, the lateral and levitation forces can be computed, respectively, by:

$$F_x(t_n) = l\int_S B_y(x, y, t_n)J_z(x, y, t_n)\mathrm{d}S; \tag{10a}$$

$$F_y(t_n) = l\int_S B_x(x, y, t_n)J_z(x, y, t_n)\mathrm{d}S, \tag{10b}$$

where l is the 2D model depth.

2.1.1. Determination of A_z^{EXT}, H_x^{EXT}, and H_y^{EXT}. Many different techniques can be used to compute the values of A_z^{EXT}, with the FEM being the usual choice. If the magnetic permeability (μ) is the same in all simulation domains, the FEM can be replaced by analytical equations. This is the case studied in this work, where $\mu = \mu_0$ was considered at all simulation points. It is important to mention that this choice does not mean that the FEM cannot be used. Solving the problem in this way allows the simulation domain, and consequently the computation time, to be reduced.

Here, the magnetic field produced by the PM in the superconductor domain was modeled by two surface current densities flowing in opposite directions. The surface current, in $\mathrm{A\ m^{-1}}$, must have the same absolute value of PM magnetization (M). This approximation is illustrated in figure 2 and is only possible due to the linear behavior of the simulation domain. For the sake of readability, we define here some distances considering $P_1(x_1, y_1, z_1)$ and an arbitrary point $P_k(x, y, z)$:

- $\Delta x_{1k} = x_1 - x$;
- $\Delta y_{1k} = y_1 - y$;
- $\Delta z_{1k} = z_1 - z$;
- $R_{1k} = \sqrt{\Delta x_{1k}^2 + \Delta y_{1k}^2 + \Delta z_{1k}^2}$;
- $r_{1k} = \sqrt{\Delta x_{1k}^2 + \Delta y_{1k}^2}$.

For the SMB presented in figure 2, the magnetic vector potential only presents non-null values in the z direction: $\mathbf{A} = (0, 0, A_z)$. The A_z value at point P_1 can be obtained by the Biot–Savart law [20]:

$$A_z^{\mathrm{EXT}}(P_1) = \frac{\mu_0 M}{4\pi}\left[\int_{P_2}^{P_3}\int_{-\infty}^{\infty}\frac{\mathrm{d}z\,\mathrm{d}y}{R_{1k}} - \int_{P_4}^{P_5}\int_{-\infty}^{\infty}\frac{\mathrm{d}z\,\mathrm{d}y}{R_{1k}}\right]. \tag{11}$$

Integrating equation (11) with respect to z results in:

$$A_z^{\mathrm{EXT}}(P_1) = \frac{\mu_0 M}{4\pi}\left[\int_{P_4}^{P_5}\ln(r_{1k}^2)\,\mathrm{d}y - \int_{P_2}^{P_3}\ln(r_{1k}^2)\,\mathrm{d}y\right]. \tag{12}$$

In the sequence, we have integrated equation (12) in the y direction for the case presented in figure 2: $x_2 = x_3$, $x_4 = x_5$, $y_2 = y_4$ and $y_3 = y_5$. The A_z value can be determined by:

$$\begin{aligned} A_z^{\mathrm{EXT}}(P_1) = \frac{\mu_0 M}{2\pi}\Bigg\{ & \frac{\Delta y_{12}}{2}\ln\left[\frac{\Delta x_{14}^2 + \Delta y_{12}^2}{\Delta x_{12}^2 + \Delta y_{12}^2}\right] \\ & + \Delta x_{14}\left[\mathrm{atan}\left(\frac{\Delta y_{12}}{\Delta x_{14}}\right) - \mathrm{atan}\left(\frac{\Delta y_{13}}{\Delta x_{14}}\right)\right] \\ & + \Delta x_{12}\left[\mathrm{atan}\left(\frac{\Delta y_{13}}{\Delta x_{12}}\right) - \mathrm{atan}\left(\frac{\Delta y_{12}}{\Delta x_{12}}\right)\right] \\ & - \frac{\Delta y_{13}}{2}\ln\left[\frac{\Delta x_{14}^2 + \Delta y_{13}^2}{\Delta x_{12}^2 + \Delta y_{13}^2}\right]\Bigg\}. \end{aligned} \tag{13}$$

Even though equation (13) is long, its value can be determined directly as a function of x_1 and y_1. This expression can be calculated without the need of a computational program, but it would result in a lot of unnecessary work. In the case where P_1 is coincident with one of the PM vertices, equation (13) would result in a singularity. However, as we are interested in the A_z value in the HTS due to the PM, it is not necessary to apply any artifice in order to eliminate these singularities.

Considering the two surface currents of values $\pm M$ [17], as shown in figure 2, it is also possible to use the Biot–Savart law to obtain [16]:

$$H_x^{\mathrm{EXT}} = \frac{M}{4\pi}\ln\frac{[\Delta y_{13}^2 + \Delta x_{13}^2][\Delta y_{14}^2 + \Delta x_{14}^2]}{[\Delta y_{12}^2 + \Delta x_{12}^2][\Delta y_{15}^2 + \Delta x_{15}^2]}; \tag{14a}$$

$$\begin{aligned} H_y^{\mathrm{EXT}} = & \frac{M}{2\pi}\mathrm{atan}\left(\frac{\Delta y_{12}}{\Delta x_{12}}\right) - \frac{M}{2\pi}\mathrm{atan}\left(\frac{\Delta y_{13}}{\Delta x_{13}}\right) \\ & - \frac{M}{2\pi}\mathrm{atan}\left(\frac{\Delta y_{14}}{\Delta x_{14}}\right) + \frac{M}{2\pi}\mathrm{atan}\left(\frac{\Delta y_{15}}{\Delta x_{15}}\right). \end{aligned} \tag{14b}$$

2.1.2. Determination of A_z^{HTS}, H_x^{HTS}, and H_y^{HTS}. In many cases, the source of the magnetic field is a conductor with an applied current. Getting straight to the point, the current induced in the HTS also changes the magnetic field inside the superconductor sample. Thus, it is very important to take this influence into account in the simulations. However, while the magnetic field produced by an external source (A_z^{EXT}, H_x^{EXT} and H_y^{EXT}) is constant in each time instant, the magnetic field component due to the induced currents in the HTS must be updated in iterative steps. In this section, we present an efficient way of computing A_z^{HTS}, H_x^{HTS} and H_y^{HTS} using analytical equations. Later on in this manuscript, we are going to discuss the advantages of using analytical equations instead of the FEM, as is the case in several studies in the literature [10, 11].

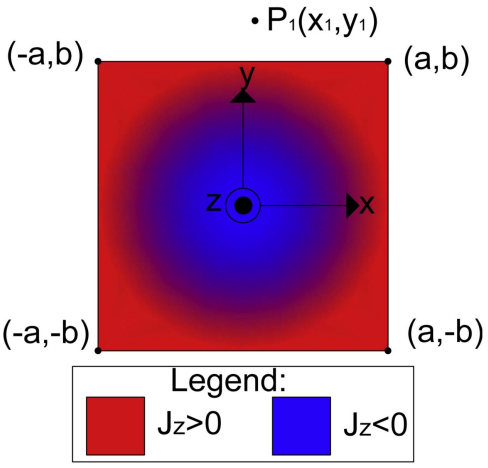

Figure 3. The current density distribution in the cross-sectional area of a conductor with longitudinal symmetry.

Consider that a current I is applied in an infinitely long conductor, whose cross-sectional area is presented in figure 3. The current density profile must be consistent with the Maxwell equations in all the simulation domains. The A_z value in point P_1 produced by the currents flowing through the HTS can be determined by equation (15)

$$A_z^{\mathrm{HTS}}(P_1) = -\frac{\mu_0}{4\pi}\int_{-b}^{b}\int_{-a}^{a} J_z(x, y)\ln(r_{1k}^2)\,\mathrm{d}x\,\mathrm{d}y. \tag{15}$$

Now, let us consider that the cross-sectional area of figure 3 represents a differential element of area $\mathrm{d}S = 4\,a\,b$, as the ones used in the FDM. In this case, the current density must be homogeneous inside the small surface $\mathrm{d}S$. A good approximation for this case is to consider a punctual current $I = J_z \cdot \mathrm{d}S$ applied at the center of the element, here defined as point $P_e(x_e, y_e)$. It is important to mention that the center of the element is not necessarily coincident with the origin of the coordinate system. As a result, A_z can be determined at P_1 by

$$A_z^{\mathrm{HTS}}(P_1) = -\frac{\mu_0 J_z}{\pi\, a\, b}\ln(\Delta x_{1e}^2 + \Delta y_{1e}^2). \tag{16}$$

It should be noted that equation (16) presents a singularity when P_1 is coincident with the geometric center of the element ($P_1 = P_e$). For this case, equation (15) can be

used in order to avoid this singularity, resulting in:

$$A_z^{\mathrm{HTS}}(P_e) = -\frac{\mu_0 J_z}{4\pi}\left[4\,a^2 \arctan\left(\frac{b}{a}\right) + 4\,b^2 \arctan\left(\frac{a}{b}\right) - 12\,a\,b + 4\,a\,b \ln(a^2+b^2)\right]. \quad (17)$$

In analogy, it is also possible to use the Biot–Savart law to obtain:

$$H_x^{\mathrm{HTS}}(P_1) = -\frac{I}{2\pi}\frac{\Delta y_{1e}}{\Delta x_{1e}^2 + \Delta y_{1e}^2}; \quad (18)$$

$$H_y^{\mathrm{HTS}}(P_1) = \frac{I}{2\pi}\frac{\Delta x_{1e}}{\Delta x_{1e}^2 + \Delta y_{1e}^2}. \quad (19)$$

It is worth mentioning that the values of H_x and H_y due to the current in a differential element of the area must be zero at the center of the element:

$$H_x^{\mathrm{HTS}}(P_e) = H_y^{\mathrm{HTS}}(P_e) = 0. \quad (20)$$

2.1.3. Details about the implementation. Understanding how to implement the A-V formulation with FDM is a challenge that needs a lot of thought. We do not want the reader to get bored with this part before seeing the potential of this tool (unless they want to). For this reason, the numerical implementation using FDM is discussed in detail in appendix A. After that, appendix B shows how to implement the A-V formulation using FDM with symmetry.

2.2. Modeling of superconducting magnetic bearings by the H formulation

Perhaps for historical reasons, most of the studies in the literature use the A-V formulation to simulate SMB. However, in a previous work [16], it was shown that the H formulation is also suitable for this application. Here, we are going to compare the performance of both techniques. The H formulation was implemented with the aid of FEM-based commercial software COMSOL and is explained in detail in [16]. Its main advantage is its ease of use, a fact that may explain why H formulation has become the most widespread technique in the literature to simulate superconducting applications.

2.3. Homogenized HTS stacks

One of the major difficulties in modeling 2G HTS wires is their high aspect ratio. The easiest way to overcome this challenge is to increase the aspect ratio of the mesh elements, which also reduces the quality of the results [21]. In some applications, like the 2G HTS stacks simulated in this work, the use of mapped meshes is not enough to reduce the large number of unknowns to something computationally feasible. The use of homogenized stacks is an alternative that can be used to overcome the aforementioned challenges [9, 22]. This technique is a geometry approximation that replaces the 2G stack with bulk superconductors, as illustrated in figure 4. However, replacing the 2G stack with a single bulk (figure 4(b)) is not advised, since it will result in a very different current density profile. Another possibility allows the user to choose the number of 2G wire segments to be embedded into each of the N_D bulk subdomains (figure 4(c)). The decision must be made by weighing the importance of a small amount of computational time (N_D small) and the accuracy of the current density profile (N_D large).

The superconducting properties of the homogenized bulk must be the same as that of the 2G stack, but rescaled to the new cross section area. As an example, the 2G wire J_c value must be replaced by an engineering critical current density (J_{ce}):

$$J_{ce}(H) = J_c(H)\, f_{\mathrm{HTS}}, \quad (21)$$

where f_{HTS} is the ratio between the cross-sectional areas of the 2G stack and of the homogenized bulk.

2.4. Experimental procedures

Some experimental measurements were performed for comparison with the results evaluated by A-V and H formulations. A schematic of the experimental setup is presented in figure 5. The experiment was done by measuring the levitation force between the PM and the HTS using a six-axis load cell model Delta-660 SI-60 [23]. A one-step motor was used to perform vertical displacements by moving the blue structure. The force resolution in the y direction is 0.25 N. The data was acquired at a sample rate of 10 kS s^{-1} and it is subject to noise due to the mechanical vibration present in the system during its displacement. To minimize this problem, the measurements were done quasi-statically, by moving the system at a speed of 0.5 mm s^{-1} along the y axis. Each of the 1000 readings were stored and averaged, so that a levitation force value was computed every 0.1 s. Each test was performed twice, with and without liquid nitrogen (LN_2). In order to cancel any measured force value not produced by the induced currents in the superconductor, measurements without LN_2 were subtracted from the ones with it.

2.4.1. Cases studied. In order to compare the simulated results calculated by the A-V and the H formulations with the measurements, we have performed a set composed of ten different tests. In all of them, Nd-Fe-B PM with dimensions of 50 mm × 50 mm × 100 mm, respectively, in the x, y, and z directions was used to produce the external magnetic field applied to the HTS. The PM coercive force was 780 kA m^{-1} and its relative magnetic permeability was set to $\mu_r = 1$. Two HTS samples were used for the tests:

- **For tests 01 to 05** an YBCO bulk was used, with dimensions of 14 mm × 34 mm × 67 mm, respectively, in the directions x, y, and z. This sample was manufactured by ATZ [24] and it presents three domains.
- **For tests 06 to 10** a stack of 2G wire was used, composed of 30 pieces divided into 3 columns with 10 segments each. The three columns are disposed side by side in the x

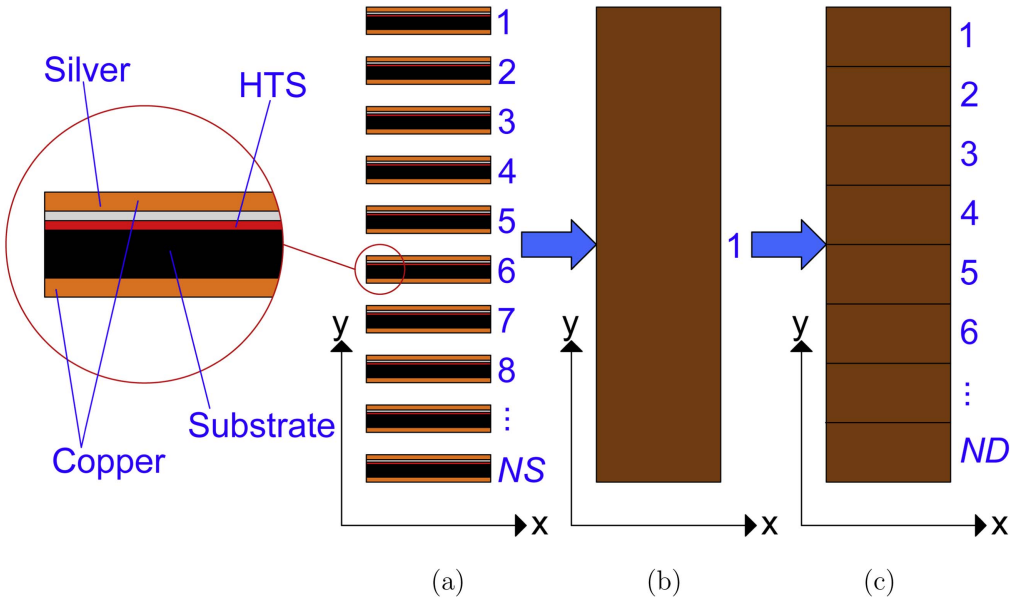

Figure 4. Illustration of the homogenization process: (a) stacked pieces of 2G N_S wire; (b) bulk superconductor; (c) N_D bulk superconductors.

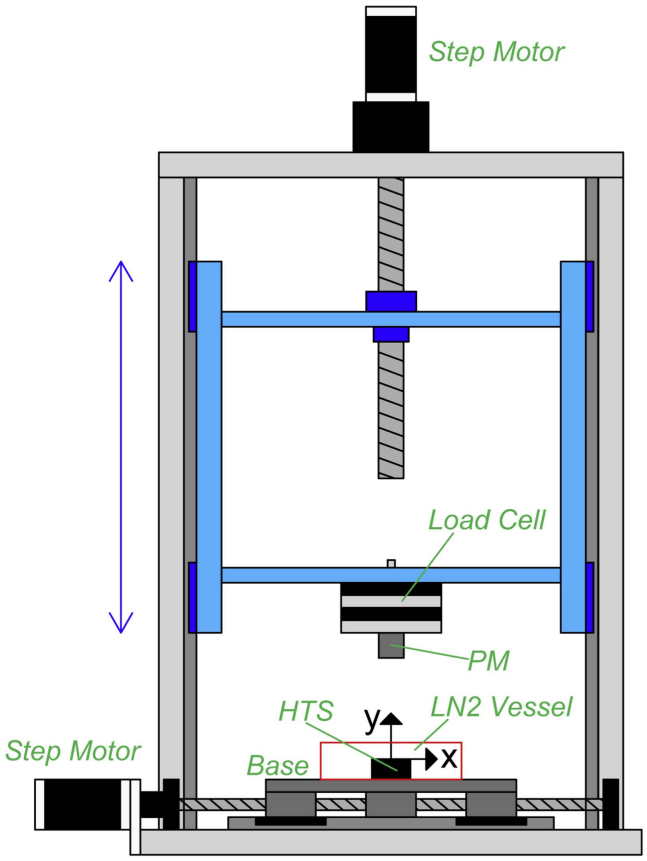

Figure 5. An illustration of the experimental rig built to measure forces in an SMB.

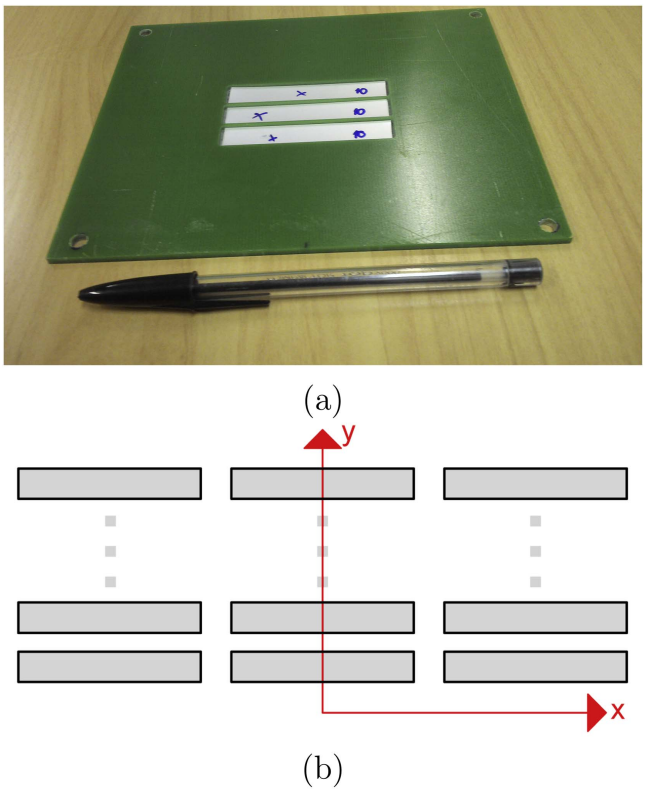

Figure 6. The three parallel 2G stacks used for the measurement system: (a) a picture and (b) an illustration of the cross-sectional area (not to scale).

direction, while pieces of 2G wire are stacked in the y direction, as presented in figure 6. Each wire segment is 67 mm in length in the z direction. The coated conductor used for these tests is model SF12050 from SuperPower [25].

Figure 7 summarizes the movements and the relative distances between the HTS samples and the PM. Tests 01 and 06 were used to adjust the parameters of the model that describe the HTS properties. The same parameters were used in the simulation of the other tests.

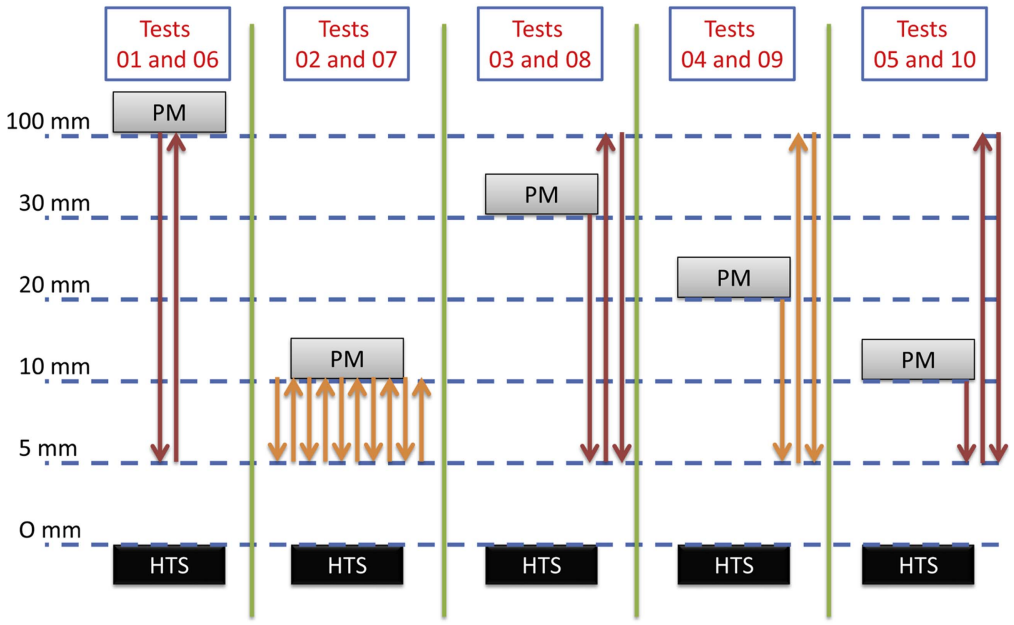

Figure 7. The distances between the permanent magnet and the HTS samples in all tests performed.

3. Results

This section presents a comparison between the measured and simulated levitation force (F_y) results for the ten tests belonging to our case studies. The quality of the results achieved with both formulation techniques (A-V and H) was evaluated by the normalized maximum error equation, which is defined as [16]:

$$\mathrm{ERR} = \frac{\max(|F_y^{\mathrm{sim}} - F_y^{\mathrm{mea}}|)}{\max(|F_y^{\mathrm{mea}}|)}, \tag{22}$$

where F_y^{sim} is a vector that stores all the simulated results, F_y^{mea} is a vector that stores all measured results and the function 'max' returns the maximum value of a vector.

All simulations in this paper were performed on a personal computer with the following settings:

- Manufacturer: DELL Inc
- Model: XPS 8300
- System type: x64
- Processor: Intel Core i7-2600 @ 3.40 GHz
- Physical memory (RAM) installed: 8.00 GB
- Software: COMSOL version 4.4.

Levitation force results are usually plotted in a force versus distance graphic. For the sake of visibility, the levitation force will be presented in the next sections using an unconventional format: force versus time. Since the relative movement between HTS and PM was performed at a fixed velocity, we do know the distance between them at each time instant. To make it easier for the reader, the distance versus time curve will also be presented.

Table 1. The parameters used in equations (8) and (9a) to model the HTS properties during tests 01–05.

Param.	Unit	Tests 1–5
E_c	V m^{-1}	$1.0 \cdot 10^{-4}$
n	⋯	$2.1 \cdot 10^{1}$
J_{c0}	A m^{-2}	$3.7 \cdot 10^{8}$
H_J	A m^{-1}	$1.8 \cdot 10^{5}$

3.1. Results for the bulk: tests 01 to 05

In these tests, the bulk superconductor properties were modeled using equations (8) and (9a) with a fixed value of the exponent n. Here test 01 was used to adjust the parameters J_{c0}, n, and H_J in order to fit the measured and the simulated results. Table 1 presents the chosen values for those parameters after the fitting procedure.

Before presenting the results, we still need to talk about some simulation settings. Since the A-V and H formulation are very different techniques, these settings do not have a direct correlation. However, the reader will not be able to reproduce the results in this manuscript without this information:

- **Settings of the A-V formulation:**
  Absolute error (ε_E) in V m^{-1}: 1e-6
  Element width ($2a$) in m: 50e-6
  Element height ($2b$) in m: 50e-6
  Number of elements (N): 952
- **Settings of the H formulation in COMSOL:**
  Absolute error in H m^{-1}: 1e-3
  Relative error: 1e-4
  Mesh refinement: 'fine'
  Number of elements (N): 896

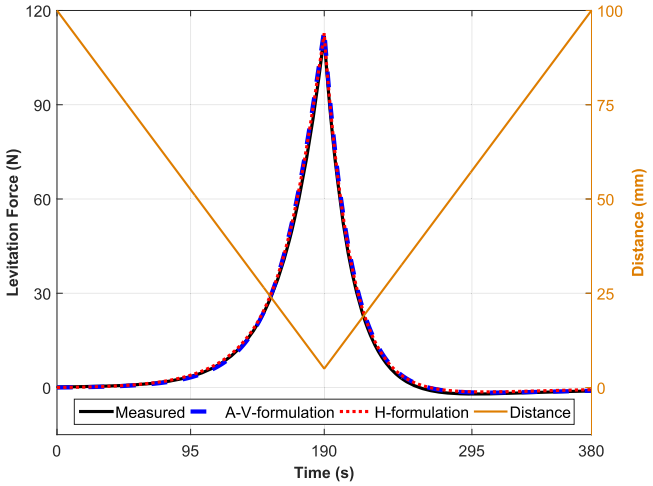

Figure 8. Test 01: measured and simulated results.

A comparison between the measured and simulated levitation forces for the H and the A-V formulations is presented in figure 8, for test 01, which represents a zero-field cooling case. Visually, in figure 8 it is difficult to distinguish which model presents better convergence, since both formulations are able to describe the phenomena very well. The maximum errors presented by the A-V and for H formulations were 3.95% and 3.22%, respectively. In terms of time, processing the A-V formulation was faster, taking 589.2 s against 808.1 s compared to H.

Figure 9 presents a comparison between the current density profile achieved with both formulations at the time instant $t = 190$ s, which corresponds to the minimum distance between the PM and HTS sample in test 01. Despite the fact that the meshes are not the same, the current density profile was very similar.

Using the same YBCO bulk parameters adjusted for test 01, we have simulated tests 02 to 05. Test 02 presents five cycles of movements for the YBCO and the PM. The sample was field-cooled with a 10 mm gap and the vertical position was reduced to 5 mm. After this, the movement was repeated four more times. The results are presented in figure 10. The parameter ERR is 4.09% for the A-V formulation, against 4.48% for the H one, with the A-V reaching the solution faster (452.4 s against 537.9 s for H).

We also investigated the application of the A-V and the H formulations to solve several field cooling gaps: test 03–30 mm, test 04–20 mm and test 05–10 mm, as presented in figure 7. It is well known that an HTS can trap part of the field when it is cooled in the presence of an external magnetic field. In relation to the trapped field produced by a permanent magnet in an HTS bulk, when the cooling distance between them is smaller, normally the superconductor can trap more flux in its interior, resulting in a reduction of the induced current during the movement. Consequently, the levitation force is reduced and the superconductor can present a more lateral force, which is not considered in this work. For both formulations, it can be observed that the maximum error during each simulation

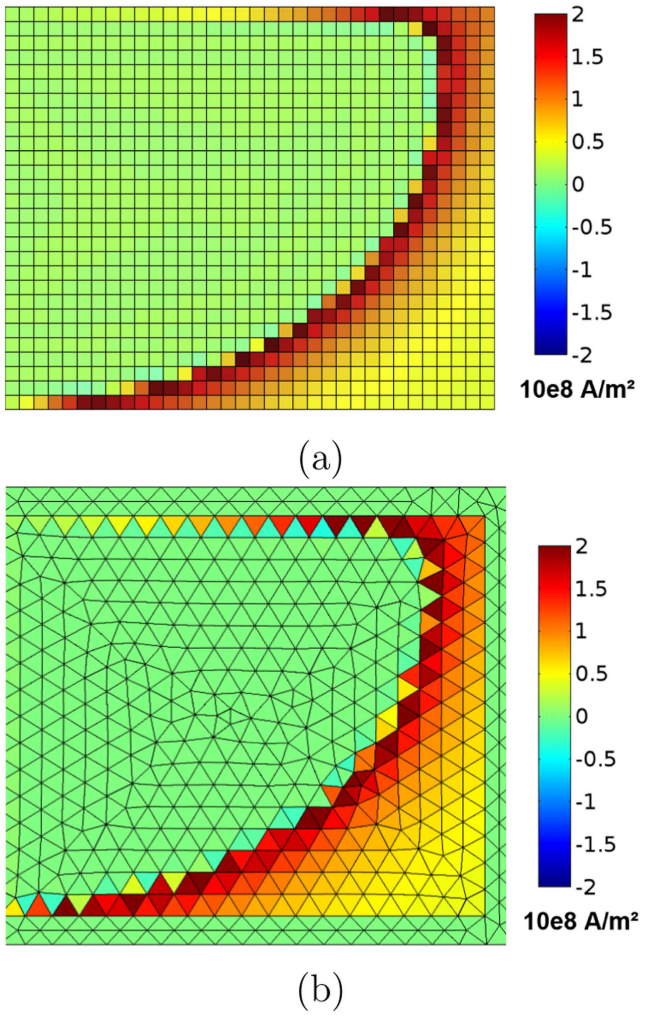

Figure 9. The simulated current density profiles for test 01 at the time instant $t = 190$ s using: (a) the A-V formulation, and (b) the H formulation.

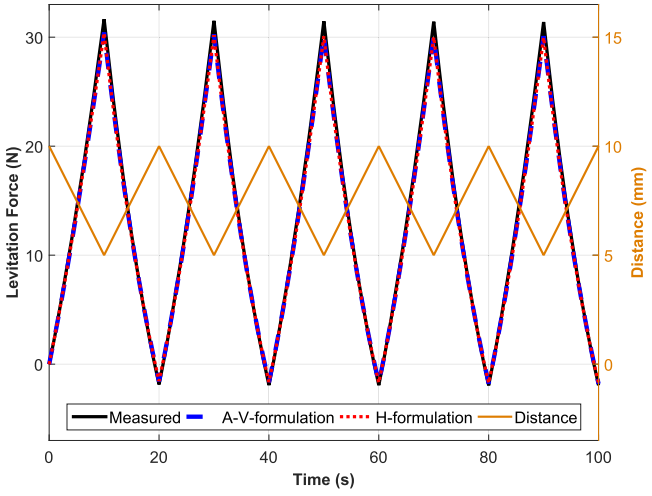

Figure 10. Test 02: measured and simulated results.

increases as the initial distance between the magnet and the superconductor decreases, as summarized in table 2. Figure 11 presents the measured and simulated results of test 03.

Table 2. Summary of tests 01 to 05.

Test	Formulation	Time (s)	ERR (%)
01	AV	589.2	3.95
	H	808.1	3.22
02	AV	452.4	4.09
	H	537.9	4.48
03	AV	737.5	3.19
	H	523.2	3.68
04	AV	663.3	6.34
	H	589.5	7.25
05	AV	583.1	13.0
	H	434.0	13.1

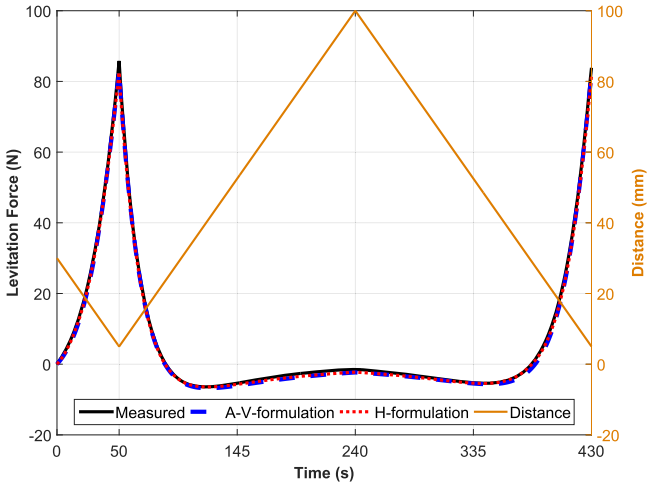

Figure 11. Test 03: measured and simulated results.

In summary, the A-V and H formulations present similar but different results. We consider it quite impressive that both techniques achieved the same magnitude of error and computation time.

3.2. Results for the 2G stack: tests 06 to 10

This section led us to the next level of SMB modeling. The YBCO bulk was replaced by stacks of 2G wire, which has highly nonlinear behavior. In addition, the high aspect ratio in the cross-sectional area of the superconduction layer in each tape needs a mesh with a large number of elements to ensure the quality of the results. As discussed in [16], the use of mapped meshes is not enough to turn the long computational time into something feasible. In this work, the problem was overcome by replacing each stack with two homogenized bulk superconductors ($N_D = 2$).

Considering the use of a symmetry axis, figure 1 shows exactly how this SMB looks after being homogenized. Each of the four bulk subdomains was meshed with one triangular element along its thickness and with 2 div mm^{-1} along the width. Keeping the same 'relative error' and 'absolute error' values of tests 01 to 05, test 06 was used to adjust the HTS properties with equations (8), (9a) and (9b). Table 3 presents the chosen values for those parameters after the fitting procedure. It is important to note that in the 2G stack case, we were only able to reproduce experimental results after introducing the exponential behavior of the n exponent, presented in equation (9b). Despite this, the reader will see that the simulation of tests 06 to 10 presents higher values of ERR when compared to tests 01 to 05 (see table 4). This means that the chosen model to describe the 2G stack properties is not as precise as the one chosen to represent the YBCO bulk.

Table 3. Parameters used in equations (8), (9a) and (9b) to model the HTS properties during tests 06 to 10.

Param.	Unit	Tests 1–5
E_c	V m^{-1}	$1.0 \cdot 10^{-4}$
J_{c0}	A m^{-2}	$3.0 \cdot 10^{8}$
n_0	⋯	$2.5 \cdot 10^{1}$
H_J	A m^{-1}	$1.2 \cdot 10^{6}$
H_n	A m^{-1}	$1.4 \cdot 10^{5}$

Table 4. Summary of tests 06 to 10.

Test	Formulation	Time (s)	ERR (%)
06	AV	170.1	8.53
	H	437.1	3.95
07	AV	279.3	19.1
	H	239.5	19.0
08	AV	300.8	9.57
	H	329.2	9.11
09	AV	305.0	9.56
	H	297.4	9.18
10	AV	247.4	12.9
	H	236.2	11.9

Figure 12 shows a comparison of the measured and simulated results for test 06. Graphically, it is hard to see any difference between the results achieved with the H and A-V formulations. However, table 4 shows that the H formulation presents a smaller value of ERR. This was expected because the fitting procedure was performed with an H formulation. What was not expected was such a difference between the ERR parameter achieved with both formulations. It is worth mentioning that in this range of levitation force, any small difference between the measured and simulated results contributes significantly to the increase of the ERR parameter, a fact which shows the high sensitivity of the metric adopted for comparisons in this manuscript.

Figure 13 shows that in test 07 the levitation error increases with each cycle of movement. This fact is due to a less accurate model in the operational range (5 mm $\leqslant$ distance $\leqslant$ 10 mm).

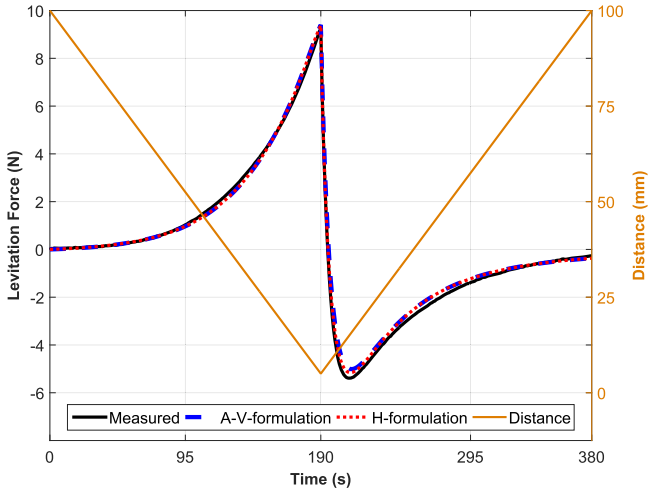

Figure 12. Test 06: measured and simulated results.

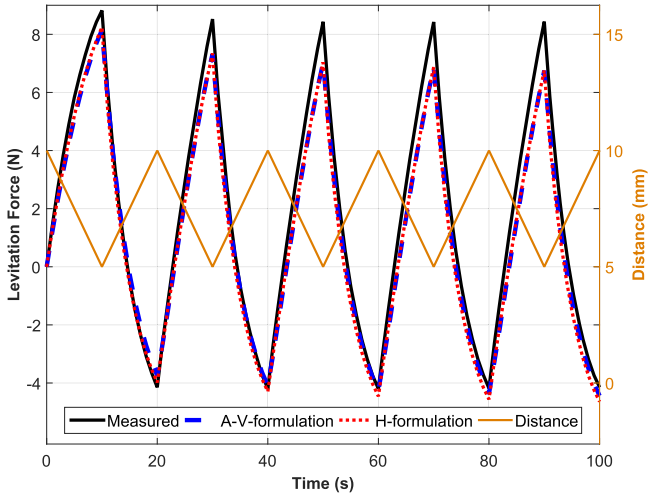

Figure 13. Test 07: measured and simulated results.

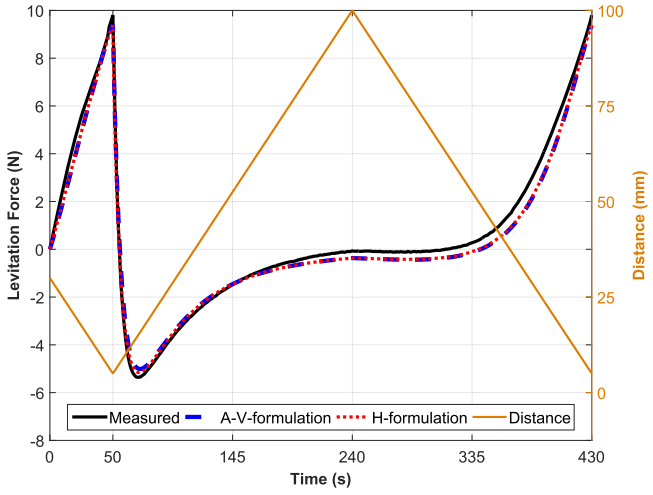

Figure 14. Test 08: measured and simulated results.

It is important to mention that we have tested several different models that can be found in the literature [19] to describe the HTS behavior, but none of them fit the electrical properties perfectly, especially for 2G wires. Still, both formulations were able to predict the behavior of the levitation force measured in test 07.

Finally, figure 14 shows that both A-V and H formulations were able to predict the SMB behavior under field-cooled conditions. More than that, both techniques achieved the same magnitude of error and computational time.

4. Conclusions

There are several studies in the literature about the simulation of SMB, and most of them use the A-V formulation. However, in a previous work [16], it was shown that the H formulation is also suitable for this propose, achieving good results when compared to the experimental data. In both cases, a reduced domain was used, eliminating the need of a moving mesh, and the movement between PM and HTS samples (one YBCO bulk and a 2G HTS stack) was represented in the boundary conditions. To carry out the tests, an experimental rig was used to measure the levitation force and to perform the movements according to the pre-established cycles that consist of five different tests. The results for both formulations presented very similar results in all cases analyzed in this work. The computational time was also in the same range of magnitude, a fact that was only possible due to improvements we presented to compute analytically some of the pre-processing matrices needed in the A-V formulation.

Considering the formulations presented in this work, one can say that the first obvious advantage of using the A-V formulation instead of the H formulation is to avoid using proprietary software. In addition, writing your own simulation code is the best way to understand and possibly solve any convergence problem. In complex models, you will be able to create any coupling that you want. If this statement is not enough to turn you into an A-V formulation user, let us talk about the unexplored potential of this tool: on the one hand, the proprietary software is a commercial tool that has been developed by an experienced team over several years. On the other hand, our code to implement the A-V formulation is quite modest and can be improved in many ways.

In summary, our contribution to A-V formulation places it at the same level of H formulation in terms of computational time and the quality of the results. We believe that full understanding of the method and complete access to each stage of the solution process, together with the independence from proprietary software, represent great advantages for the presented A-V formulation technique.

Acknowledgments

The authors would like to thank the Brazilian agencies CNPq and FAPERJ for financially supporting the research.

Appendix A. Numerical implementation of the A-V formulation using the FDM

Applying the implicit FDM in equation (7) results in:

$$\rho\, J_z^{t_n} = -\frac{A_{z_{\mathrm{EXT}}}^{t_n} - A_{z_{\mathrm{EXT}}}^{t_n-\Delta t}}{\Delta t} - \frac{A_{z_{\mathrm{HTS}}}^{t_n} - A_{z_{\mathrm{HTS}}}^{t_n-\Delta t}}{\Delta t} - C^{t_n}. \tag{A.1}$$

Here, we present a numerical procedure to solve equation (A.1) in each element of the domain.

The FDM needs spatial discretization of the superconductor geometry. In the present work, the used elements are rectangles with width $2\,a$ and height $2\,b$. Figure A1 presents the HTS divided in m lines and k columns, resulting in a total of $N = k \cdot m$ elements. Each element receives a number, which is used for its identification. Since the external influences are computed by analytical equations, the simulation domain is composed exclusively of the HTS.

Besides the spatial discretization, time discretization of the problem is also necessary. Here, the system of equations was solved using fixed time step intervals (Δt), predefined by the user, between the initial time ($t = 0$) and the final simulation time ($t = t_{\mathrm{final}}$). Let us consider D as the number of simulated time instants, so that the vector $[t]_{1\times D}$ can be defined as:

$$[t]_{1\times D} = \begin{bmatrix} 0\ \Delta t & 1\ \Delta t & \cdots & t_{\mathrm{final}} = (D-1)\Delta t \end{bmatrix} = [\, t^{(1)} \quad t^{(2)} \quad \cdots \quad t^{(D)}]. \tag{A.2}$$

The current density in each one of the N elements presented in figure A1 should be computed for all time instants during the HTS movement. The results must be saved for later use in post-processing: computation of the lateral and levitation forces. In order to do this, each column of the matrix $[J_z]_{N\times D}$ stores the current density values for a determined time instant. The rows of this matrix are responsible for storing the current density values of a single element.

$$[J_z]_{N\times D} = \begin{bmatrix} J_z^{(1,1)} & J_z^{(1,2)} & \cdots & J_z^{(1,D)} \\ J_z^{(2,1)} & J_z^{(2,2)} & \cdots & J_z^{(2,D)} \\ \vdots & \vdots & \ddots & \vdots \\ J_z^{(N,1)} & J_z^{(N,2)} & \cdots & J_z^{(N,D)} \end{bmatrix} = \begin{bmatrix} [J_z]_{N\times 1}^{t^{(1)}} & [J_z]_{N\times 1}^{t^{(2)}} & \cdots & [J_z]_{N\times 1}^{t^{(D)}} \end{bmatrix}. \tag{A.3}$$

In analogy, using the same notation as equations (A.2) and (A.3), here we define:

- $[x_{\mathrm{elem}}]_{N\times D}$ and $[y_{\mathrm{elem}}]_{N\times D} \Longrightarrow$ matrices to store, respectively, the values of x_{elem} and y_{elem} in each element and in each time instant. These matrices are responsible for defining the HTS movement in relation to the PM, and for this reason must be defined during pre-processing;

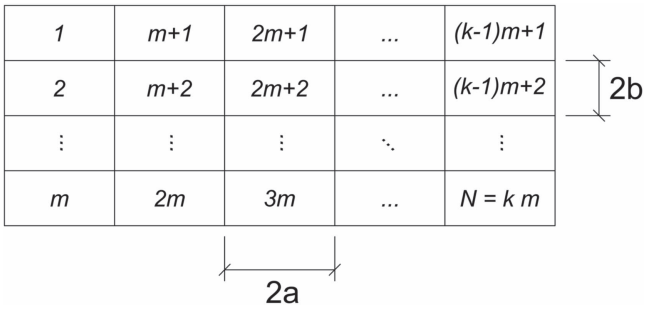

Figure A1. The HTS spatial discretization in the $N = k \cdot m$ rectangular elements with width $2\,a$ and height $2\,b$.

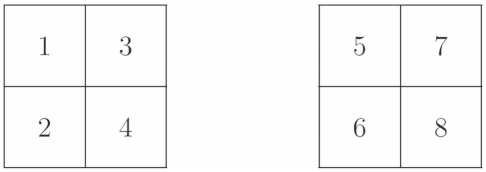

Figure A2. The elements of two superconducting domains ($NS = 2$).

- $[A_{z_{\mathrm{EXT}}}]_{N\times D}$, $[H_{x_{\mathrm{EXT}}}]_{N\times D}$ and $[H_{y_{\mathrm{EXT}}}]_{N\times D} \Longrightarrow$ matrices to store, respectively, the values of A_z, H_x and H_y in each element and in each time instant due to the external sources of the magnetic field. These matrices must be defined during pre-processing using equations (13), (14a) and (14b);
- $[A_{z_{\mathrm{HTS}}}]_{N\times D} \Longrightarrow$ matrix to store the values of A_z in each element and in each time instant due to the induced currents in the HTS. This matrix changes as $[J_z]_{N\times 1}^{t_n}$ changes in the iterative solution process. Considering the linear magnetic properties and applying the superposition principle, [26] shows that:

$$[A_{z_{\mathrm{HTS}}}]_{N\times 1}^{t_n} = [M_{A_z}]_{N\times N}\ [J_z]_{N\times 1}^{t_n}, \tag{A.4}$$

where the matrix $[M_{A_z}]_{N\times N}$, is constant.

In the literature, $[M_{A_z}]_{N\times N}$ is usually built using the results of N FEM simulations [10, 11, 26]. This procedure is a big challenge for those learning the technique. Besides, how much time do we need to run N simulations based on FEM? In fact, this depends on how many elements discretize your domain, the size of the domain and the quality of the FEM algorithms. Here, we propose an alternative technique that uses analytical equations to speed up the process without compromising the quality of the results.

Before explaining the proposed technique to build $[M_{A_z}]_{N\times N}$, here we define i and j as two arbitrary indices to identify, respectively, the rows and columns of a matrix. Next, we apply a unitary current density ($J_z = 1\ \mathrm{A\ m^{-2}}$) in the element $i = 1$ of the HTS at the time instant $t^{(k)} = t_n$. This

allows us to rewrite equation (A.4) as:

$$\begin{bmatrix} M_{A_z}^{(1,1)} & M_{A_z}^{(1,2)} & \cdots & M_{A_z}^{(1,N)} \\ M_{A_z}^{(2,1)} & M_{A_z}^{(2,2)} & \cdots & M_{A_z}^{(2,N)} \\ \vdots & \vdots & \ddots & \vdots \\ M_{A_z}^{(N,1)} & M_{A_z}^{(N,2)} & \cdots & M_{A_z}^{(N,N)} \end{bmatrix} \begin{bmatrix} 1 \\ 0 \\ \vdots \\ 0 \end{bmatrix} = \begin{bmatrix} M_{A_z}^{(1,1)} \\ M_{A_z}^{(2,1)} \\ \vdots \\ M_{A_z}^{(N,1)} \end{bmatrix} = \begin{bmatrix} A_{z_{\mathrm{HTS}}}^{(1,k)} \\ A_{z_{\mathrm{HTS}}}^{(2,k)} \\ \vdots \\ A_{z_{\mathrm{HTS}}}^{(N,k)} \end{bmatrix}. \tag{A.5}$$

The result presented in equation (A.5) is the first column of the matrix $[M_{A_z}]_{N\times N}$. As an example, the element $M_{A_z}^{(i,j)}$ is the value of A_z in the element j when $J_z = 1$ A m^{-2} is applied in element i. Equations (16) and (17) can be used to compute these values. It is important to note that $M_{A_z}^{(i,j)} = M_{A_z}^{(j,i)}$. Another column of $[M_{A_z}]_{N\times N}$ can be determined by applying a unitary current density in element $i = 2$, as exemplified next:

$$\begin{bmatrix} M_{A_z}^{(1,1)} & M_{A_z}^{(1,2)} & \cdots & M_{A_z}^{(1,N)} \\ M_{A_z}^{(2,1)} & M_{A_z}^{(2,2)} & \cdots & M_{A_z}^{(2,N)} \\ \vdots & \vdots & \ddots & \vdots \\ M_{A_z}^{(N,1)} & M_{A_z}^{(N,2)} & \cdots & M_{A_z}^{(N,N)} \end{bmatrix} \begin{bmatrix} 0 \\ 1 \\ \vdots \\ 0 \end{bmatrix} = \begin{bmatrix} M_{A_z}^{(1,2)} \\ M_{A_z}^{(2,2)} \\ \vdots \\ M_{A_z}^{(N,2)} \end{bmatrix} = \begin{bmatrix} A_{z_{\mathrm{HTS}}}^{(1,k)} \\ A_{z_{\mathrm{HTS}}}^{(2,k)} \\ \vdots \\ A_{z_{\mathrm{HTS}}}^{(N,k)} \end{bmatrix}. \tag{A.6}$$

This procedure must be repeated until all columns of $[M_{A_z}]_{N\times N}$ are determined. This leads us to the following conclusion:

$$M_{A_z}^{(i,j)} = M_{A_z}^{(j,i)} \Rightarrow \begin{cases} \text{Equation(16)} \Leftrightarrow i \neq j \\ \text{Equation(17)} \Leftrightarrow i = j \end{cases}. \tag{A.7}$$

To achieve a consistent matricial system, the resistivity of each element is represent by the diagonal matrix $[\rho]_{N\times N}$:

$$[\rho]_{N\times N} = \begin{bmatrix} \rho^{(1)} & 0 & \cdots & 0 \\ 0 & \rho^{(2)} & \cdots & 0 \\ \vdots & \vdots & \ddots & \vdots \\ 0 & 0 & 0 & \rho^{(N)} \end{bmatrix}, \tag{A.8}$$

where $\rho^{(i)}$ can be computed by equation (8), so that its value depends on $J_z^{(i,1)}$. In this way, $[\rho]_{N\times N}$ must be updated in every iteration of the solution process. As presented in equations (9a) and (9b), we considered that J_c and the exponent n are dependent on the magnetic field. The procedure to compute the magnetic field components is analogous to the one described to compute A_z:

$$\begin{cases} [H_x]_{N\times D} = [H_{x_{\mathrm{EXT}}}]_{N\times D} + [H_{x_{\mathrm{HTS}}}]_{N\times D} \\ [H_y]_{N\times D} = [H_{y_{\mathrm{EXT}}}]_{N\times D} + [H_{y_{\mathrm{HTS}}}]_{N\times D} \end{cases}, \tag{A.9}$$

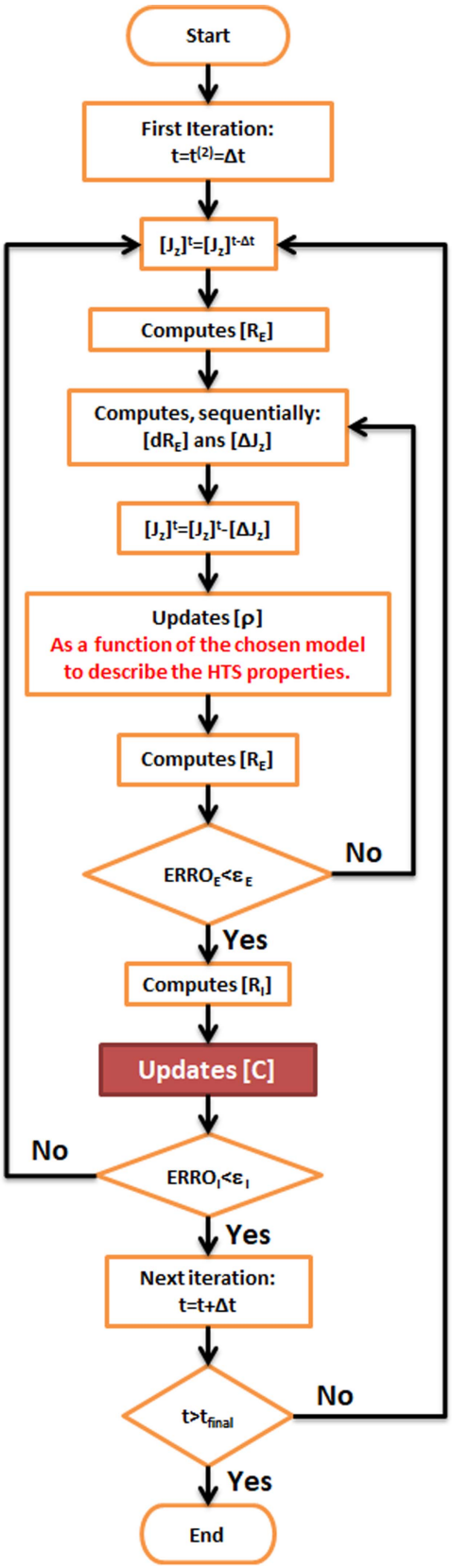

Figure A3. A block diagram of the solution algorithm.

where:

$$\begin{cases} [H_{x_{\mathrm{HTS}}}]_{N\times 1}^{t_n} = [M_{H_x}]_{N\times N}\ [J_z]_{N\times 1}^{t_n} \\ [H_{y_{\mathrm{HTS}}}]_{N\times 1}^{t_n} = [M_{H_y}]_{N\times N}\ [J_z]_{N\times 1}^{t_n} \end{cases}, \tag{A.10}$$

and:

$$\begin{cases} M_{H_x}^{(i,j)} = -M_{H_x}^{(j,i)} \Rightarrow \begin{cases} \text{Equation(18)} \Leftrightarrow i \neq j \\ 0 \Leftrightarrow i = j \end{cases} \\ M_{H_y}^{(i,j)} = -M_{H_y}^{(j,i)} \Rightarrow \begin{cases} \text{Equation(19)} \Leftrightarrow i \neq j \\ 0 \Leftrightarrow i = j \end{cases} \end{cases}. \tag{A.11}$$

In order to apply the desired net current in all superconductors, we must define each HTS domain. Consider *ND* as the number of superconducting domains. The matrix $[E_D]_{NS\times N}$ identifies the elements that belongs to each domain. At the same time, the matrix $[I]_{NS\times D}$ is responsible for storing the net current information of each HTS at all time instants:

$$[I]_{NS\times D} = 4\,a\,b[E_D]_{NS\times N}[J_z]_{N\times D}, \tag{A.12}$$

where $4\,a\,b$ is the area of the elements. To illustrate the use of equation (A.12), consider two superconducting domains and their eight elements, as shown in figure A2: elements 1 to 4 belong to domain 1, and elements 5 to 8 belong to domain 2. For this example, in an arbitrary time instant $t^{(k)} = t_n$, equation (A.12) can be written as:

$$\begin{aligned} &\begin{bmatrix} I^{(1,k)} \\ I^{(2,k)} \end{bmatrix} \\ &= 4\,a\,b\begin{bmatrix} 1 & 1 & 1 & 1 & 0 & 0 & 0 & 0 \\ 0 & 0 & 0 & 0 & 1 & 1 & 1 & 1 \end{bmatrix}\begin{bmatrix} J_z^{(1,k)} \\ J_z^{(2,k)} \\ \vdots \\ J_z^{(8,k)} \end{bmatrix} \\ &= 4\,a\,b\begin{bmatrix} J_z^{(1,k)} + J_z^{(2,k)} + J_z^{(3,k)} + J_z^{(4,k)} \\ J_z^{(5,k)} + J_z^{(6,k)} + J_z^{(7,k)} + J_z^{(8,k)} \end{bmatrix}. \end{aligned} \tag{A.13}$$

We should note that $[E_D]_{NS\times N}$ is only composed of ones and zeros, indicating whether element j belongs to domain i or not. For the sake of readability, the transpose of matrix $[E_D]_{NS\times N}$ will be called $[E_D]^{\text{Trans}}_{N\times NS}$.

Since we have not applied any constraint to the net current of the superconducting domains yet, the elements of $[I]_{NS\times D}$ can present any value. The desired values of the net current are stored in the matrix $[I_{TR}]_{NS\times D}$. In order to set these constraints, we must adjust the values of $[C]_{NS\times D}$, as indicated next:

$$R_I^{(i)} = I^{(i,j)} - I_{TR}^{(i,j)}\begin{cases} >0 \Rightarrow C^{(i,j)} \text{ increase} \\ <0 \Rightarrow C^{(i,j)} \text{ decrease} \end{cases}, \tag{A.14}$$

where the array $[R_I]_{NS\times 1}$ stores the net current errors in all *NS* domains. For this reason, $[R_I]_{NS\times 1}$ is a parameter to be minimized in the solution algorithm.

Finally, for the FDM implementation, equation (A.1) can be rewritten as:

$$\begin{aligned} [\rho]_{N\times N}[J_z]^{t_n}_{N\times 1} = &-\frac{[M_{A_z}]_{N\times N}[J_z]^{t_n}_{N\times 1}}{\Delta t} \\ &+ \frac{[M_{A_z}]_{N\times N}[J_z]^{t_n-\Delta t}_{N\times 1}}{\Delta t} \\ &- \frac{[A_{z_{\text{EXT}}}]^{t_n}_{N\times 1}}{\Delta t} + \frac{[A_{z_{\text{EXT}}}]^{t_n-\Delta t}_{N\times 1}}{\Delta t} \\ &- [E_D]^{\text{Trans}}_{N\times NS}[C]^{t_n}_{NS\times 1} \end{aligned} \tag{A.15}$$

where $[E_D]^{\text{Trans}}_{N\times NS}[C]^{t_n}_{NS\times 1}$ is an array with N elements. In order to minimize the net current error in the time instant $t^{(k)} = t_n$, this array adds the constant $C^{(i,k)}$ to all elements that belong to domain i.

Equation (A.15) equals the electric field obtained by the power law (left-hand side) to the one obtained by the A-V formulation (right-hand side). In order to solve this equation using the method of Newton–Raphson, we have rearranged equation (A.15) to create a residual error parameter ($[R_E]_{N\times 1}$) to be minimized

$$\begin{aligned} [R_E]_{N\times 1} = &\left([\rho]_{N\times N} + \frac{[M_{A_z}]_{N\times N}}{\Delta t}\right)[J_z]^{t_n}_{N\times 1} \\ &- \frac{[M_{A_z}]_{N\times N}}{\Delta t}[J_z]^{t_n-\Delta t}_{N\times 1} \\ &+ \frac{[A_{z_{\text{EXT}}}]^{t_n}_{N\times 1}}{\Delta t} - \frac{[A_{z_{\text{EXT}}}]^{t_n-\Delta t}_{N\times 1}}{\Delta t} \\ &+ [E_D]^{\text{Trans}}_{N\times NS}[C]^{t_n}_{NS\times 1}. \end{aligned} \tag{A.16}$$

The Newton–Raphson method finds the values of $[J_z]^{t_n}_{N\times 1}$ that minimize the electric field errors stored in $[R_E]_{N\times 1}$. In order to do this, we need to define $[\mathrm{d}R_E]_{N\times 1}$:

$$\begin{aligned} [\mathrm{d}R_E]_{N\times 1} &= \frac{\partial [R_E]_{N\times 1}}{\partial [J_z]^{t_n}_{N\times 1}} \\ &= \left([\rho]_{N\times N} + \frac{[M_{A_z}]_{N\times N}}{\Delta t}\right)[U]_{N\times 1}, \end{aligned} \tag{A.17}$$

where the array $[U]_{N\times 1}$ is only composed of unitary elements:

$$[U]_{N\times 1} = \begin{bmatrix} 1 \\ 1 \\ \vdots \\ 1 \end{bmatrix}. \tag{A.18}$$

With equations (A.16) and (A.17), we can compute $[\Delta J_z]_{N\times 1}$, which is an array that represents how much the elements of $[J_z]^{t_n}_{N\times 1}$ change their values at each iteration

$$[\Delta J_z]_{N\times 1} = \begin{bmatrix} \dfrac{R_E^{(1,1)}}{\mathrm{d}R_E^{(1,1)}} \\ \dfrac{R_E^{(2,1)}}{\mathrm{d}R_E^{(2,1)}} \\ \vdots \\ \dfrac{R_E^{(N,1)}}{\mathrm{d}R_E^{(N,1)}} \end{bmatrix}. \tag{A.19}$$

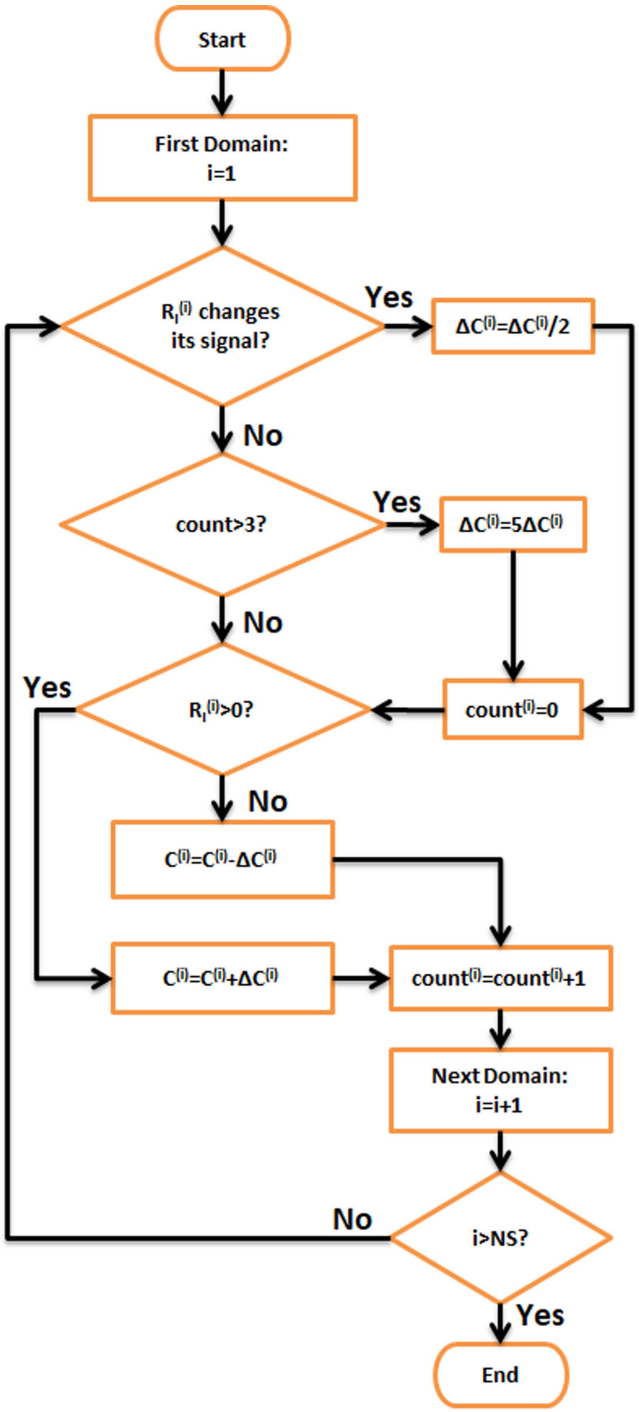

Figure A4. A block diagram of the function 'update $[C]$'.

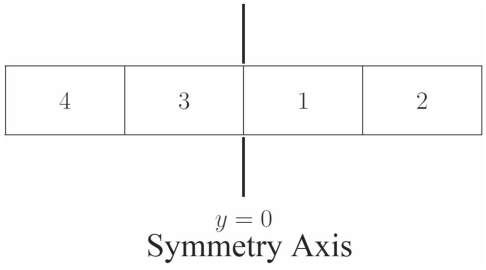

Figure B1. An example of the spatial discretization of an HTS domain with symmetry.

Finally, according to the Newton–Raphson method, the current density in the elements is updated at each iteration:

$$[J_z]^{t_n}_{N\times 1} = [J_z]^{t_n}_{N\times 1} - [\Delta J_z]_{N\times 1}. \tag{A.20}$$

Convergence is achieved when the electric field and net current errors are below a specified value. This means:

$$\text{ERROR}_E = \max(|[R_E]_{N\times 1}|) < \varepsilon_E, \tag{A.21}$$

$$\text{ERROR}_I = \max(|[R_I]_{N\times 1}|) < \varepsilon_I. \tag{A.22}$$

Figure A3 presents a complete block diagram of the solution algorithm. The block 'update $[C]$' is highlighted because we still need to discuss it. Equation (A.14) shows when the elements of the array $[C]_{NS\times D}$ must increase or decrease, but it says nothing about the amount to add or subtract in each domain. Here, for an arbitrary domain i, we will call this quantity $\Delta C^{(i)}$. Using a fixed $\Delta C^{(i)}$ will lead to convergence problems. In order to avoid this, we have developed an algorithm to 'update $[C]$', which is presented in figure A4. In this algorithm, the value of $\Delta C^{(i)}$ is reduced to half every time the net current in a domain changes its signal. While the signal remains unchangeable, the same value of $\Delta C^{(i)}$ can be applied three times. After that, the next $\Delta C^{(i)}$ will be five times bigger.

Appendix B. A-V formulation using FDM with symmetry

In any simulation method, it is important to identify symmetries in order to reduce the computational time to achieve a solution. Figure B1 shows an example of the spatial discretization of an HTS domain with symmetry. In our magnetic bearing analysis, quantities on the right-hand and left-hand sides of the symmetry axis are related by:

$$A_z(x, y) = -A_z(-x, y); \tag{B.1}$$

$$H_x(x, y) = -H_x(-x, y); \tag{B.2}$$

$$H_y(x, y) = H_y(-x, y); \tag{B.3}$$

$$J_z(x, y) = -J_z(-x, y). \tag{B.4}$$

In order to add the symmetry effect in the A-V formulation implemented with FDM, we need to modify $[M_{A_z}]_{N\times N}$. The procedure to build a new matrix must consider that when a positive current flows in the right-hand side, a negative current flows in the left-hand side, as described in equation (B.4). Considering figure B1 as an example, this can be done as follows:

$$\begin{bmatrix} M_{A_z}^{(1,1)} & M_{A_z}^{(1,2)} & M_{A_z}^{(1,3)} & M_{A_z}^{(1,N)} \\ M_{A_z}^{(2,1)} & M_{A_z}^{(2,2)} & M_{A_z}^{(2,3)} & M_{A_z}^{(2,N)} \\ M_{A_z}^{(3,1)} & M_{A_z}^{(3,2)} & M_{A_z}^{(3,3)} & M_{A_z}^{(3,N)} \\ M_{A_z}^{(N,1)} & M_{A_z}^{(4,2)} & M_{A_z}^{(4,3)} & M_{A_z}^{(4,4)} \end{bmatrix} \begin{bmatrix} 1 \\ 0 \\ -1 \\ 0 \end{bmatrix}$$
$$= \begin{bmatrix} M_{A_z}^{(1,1)} - M_{A_z}^{(1,3)} \\ M_{A_z}^{(2,1)} - M_{A_z}^{(2,3)} \\ M_{A_z}^{(3,1)} - M_{A_z}^{(3,3)} \\ M_{A_z}^{(4,1)} - M_{A_z}^{(4,3)} \end{bmatrix} = \begin{bmatrix} A_{z_{\mathrm{HTS}}}^{(1,k)} \\ A_{z_{\mathrm{HTS}}}^{(2,k)} \\ A_{z_{\mathrm{HTS}}}^{(3,k)} \\ A_{z_{\mathrm{HTS}}}^{(4,k)} \end{bmatrix}. \quad \text{(B.5)}$$

Note that with this symmetry, the system needs to be solved for $N_{\mathrm{sim}} = N/2$ elements. In this way, the reduced matrix $[M_{A_z}]_{N\times N}$ is named here as $[Mr_{A_z}]_{N_{\mathrm{sim}}\times N_{\mathrm{sim}}}$ and defined by:

$$[Mr_{A_z}]_{N_{\mathrm{sim}}\times N_{\mathrm{sim}}} = \begin{bmatrix} (M_{A_z}^{(1,1)} - M_{A_z}^{(1,3)}) & (M_{A_z}^{(1,2)} - M_{A_z}^{(1,4)}) \\ (M_{A_z}^{(2,1)} - M_{A_z}^{(2,3)}) & (M_{A_z}^{(2,2)} - M_{A_z}^{(2,4)}) \end{bmatrix}. \quad \text{(B.6)}$$

In a general form, $[Mr_{A_z}]_{N_{\mathrm{sim}}\times N_{\mathrm{sim}}}$ is composed of a combination of elements from $[M_{A_z}]_{N\times N}$:

$$Mr_{A_z}^{(i,j)} = M_{A_z}^{(i,j)} - M_{A_z}^{(i,N_{\mathrm{sim}}+j)}. \quad \text{(B.7)}$$

In analogy, using the same procedure we can also compute $[Mr_{H_x}]_{N_{\mathrm{sim}}\times N_{\mathrm{sim}}}$ and $[Mr_{H_y}]_{N_{\mathrm{sim}}\times N_{\mathrm{sim}}}$. In summary, to solve a problem using symmetry, all you need to do is to replace the complete matrices with the reduced ones.

One question still remains: after solving the current density values, how to compute the levitation force defined in equation (10b)? This can be done at each time instant (t_n) by:

$$F_y(t_n) = 2l\mu_0(4ab)[H_x^{TR}]_{1\times N}^{t_n}[J_z]_{N\times 1}^{t_n}, \quad \text{(B.8)}$$

where 2 computes the contribution of both sides of the symmetry axis, l is the 2D model depth and $[H_x^{TR}]$ is the transpose matrix of $[H_x]$.

ORCID iDs

F Sass https://orcid.org/0000-0001-5920-2502

References

[1] Nishijima S *et al* 2013 Superconductivity and the environment: a roadmap *Supercond. Sci. Technol.* **26** 113001

[2] Coombs T A, Cansiz A and Campbell A M 2002 A superconducting thrust-bearing system for an energy storage flywheel *Supercond. Sci. Technol.* **15** 831

[3] Sotelo G G, de Andrade R and Ferreira A C 2007 Magnetic bearing sets for a flywheel system *IEEE Trans. Appl. Supercond.* **17** 2150–3

[4] Sotelo G G, Dias D H N, de Andrade R and Stephan R M 2011 Tests on a superconductor linear magnetic bearing of a full-scale maglev vehicle *IEEE Trans. Appl. Supercond.* **21** 1464–8

[5] Zheng B, Zheng J, He D, Ren Y and Deng Z 2016 Magnetic characteristics of permanent magnet guideways at low temperature and its effect on the levitation force of bulk {YBaCuO} superconductors *J. Alloys Compd.* **656** 81

[6] Sass F, de Castro A R, Gonalves Sotelo G and de Andrade R 2015 Persistent currents in a magnetic bearing with coated conductors *J. Appl. Phys.* **118** 203901

[7] Patel A, Hopkins S C, Baskys A, Kalitka V, Molodyk A and Glowacki B A 2015 Magnetic levitation using high temperature superconducting pancake coils as composite bulk cylinders *Supercond. Sci. Technol.* **28** 115007

[8] Hong Z, Campbell A M and Coombs T A 2006 Numerical solution of critical state in superconductivity by finite element software *Supercond. Sci. Technol.* **19** 1246

[9] Zermeno V M R, Abrahamsen A B, Mijatovic N, Jensen B B and Srensen M P 2013 Calculation of alternating current losses in stacks and coils made of second generation high temperature superconducting tapes for large scale applications *J. Appl. Phys.* **114** 173901

[10] Ruiz-Alonso D, Coombs T A and Campbell A M 2004 Numerical analysis of high-temperature superconductors with the critical-state model *IEEE Trans. Appl. Supercond.* **14** 2053–63

[11] Dias D H N, Motta E S, Sotelo G G and de Andrade R Jr 2010 Experimental validation of field cooling simulations for linear superconducting magnetic bearings *Supercond. Sci. Technol.* **23** 075013

[12] Morandi A 2012 2D electromagnetic modelling of superconductors *Supercond. Sci. Technol.* **25** 104003

[13] Lahtinen V, Lyly M, Stenvall A and Tarhasaari T 2012 Comparison of three eddy current formulations for superconductor hysteresis loss modelling *Supercond. Sci. Technol.* **25** 115001

[14] Stenvall A and Tarhasaari T 2010 Programming finite element method based hysteresis loss computation software using non-linear superconductor resistivity and $t - \varphi$ formulation *Supercond. Sci. Technol.* **23** 075010

[15] Barrett J W and Prigozhin L 2012 Electric field formulation for thin film magnetization problems *Supercond. Sci. Technol.* **25** 104002

[16] Sass F, Sotelo G G, De Andrade R and Sirois F 2015 H-formulation for simulating levitation forces acting on HTS bulks and stacks of 2G coated conductors *Supercond. Sci. Technol.* **28** 125012

[17] Ma G-T, Liu H, Li X-T, Zhang H and Xu Y-Y 2014 Numerical simulations of the mutual effect among the superconducting constituents in a levitation system with translational symmetry *J. Appl. Phys.* **115** 083908

[18] Rhyner J 1993 Magnetic properties and ac-losses of superconductors with power law current–voltage characteristics *Physica C* **212** 292–300

[19] Navau C, Del-Valle N and Sanchez A 2013 Macroscopic modeling of magnetization and levitation of hard type-II superconductors: The critical-state model *IEEE Trans. Appl. Supercond.* **23** 8201023

[20] Hayt W H and Buck J A 2009 *Engineering Electromagnetics* VII edn (New Delhi: McGraw-Hill)

[21] Rodriguez-Zermeno V M, Mijatovic N, Traeholt C, Zirngibl T, Seiler E, Abrahamsen A B, Pedersen N F and Sorensen M P 2011 Towards faster FEM simulation of thin film superconductors: A multiscale approach *IEEE Trans. Appl. Supercond.* **21** 3273–6

[22] Zermeño V M R and Grilli F 2014 3D modeling and simulation of 2G HTS stacks and coils *Supercond. Sci. Technol.* **27** 044025
[23] Ati Industrial Automation, http://ati-ia.com/products/ft/sensors.aspx (Accessed: 15 Mar 2016)
[24] Adelwitz Technologiezentrum GmbH http://atz-gmbh.com/ (Accessed: 15 Mar 2016)
[25] Superpower Inc. http://superpower-inc.com/ (Accessed: 15 Mar 2016)
[26] Ruiz-Alonso D, Coombs T and Campbell A M 2004 Computer modelling of high-temperature superconductors using an a–v formulation *Supercond. Sci. Technol.* **17** S305